Colourless luminescent solar concentrators based on Iridium(III)-Phosphors

Colourless Luminescent Solar Concentrators based on Iridium(III)-Phosphors

Valentina Fiorini,[a] Nicola Monti,[a] Giulia Vigarani,[a] Greta Santi,[b] Francesca Fasulo,[c] Massimiliano Massi,[d] Loris Giorgini,[a] Ana B. Muñoz-García,[e] Michele Pavone,[c] Andrea Pucci,[b]* and Stefano Stagni[a]*

a: Department of Industrial Chemistry "Toso Montanari", University of Bologna, Viale Del Risorgimento 4, 40126 Bologna, Italy.

b: Department of Chemistry and Industrial Chemistry, University of Pisa, Via Giuseppe Moruzzi 13, 56124 Pisa, Italy.

c: Department of Chemical Science, University of Napoli Federico II, Via Cinthia 21, 80126 Napoli, Italy.

d: Curtin Institute for Functional Molecules and Interfaces, School of Molecular and Life Science, Curtin University, Kent Street, Bentley 6102 WA, Australia.

e: Department of Physics "Ettore Pancini", University of Napoli Federico II, Via Cinthia 21, 80126 Napoli, Italy.

Email: Andrea Pucci (andrea.pucci@unipi.it); Stefano Stagni (stefano.stagni@unibo.it).

Abstract

The first real examples of luminescent solar concentrators (LSCs) based on Ir(III) cyclometalates, are described herein. Two new Ir(III) tetrazole complexes, namely **[Ir(ppy)$_2$(iQTZ-PPG)]$^+$** and **[Ir(npy)$_2$(iQTZ-PPG)]$^+$**, where (C^N) = **ppy**, 2 phenylpyridine or **npy** = 2-(naphthalen-2-yl)pyridine and **iQTZ-PPG** = 1-(2-(prop-2-yn-1-yl)-2*H*-tetrazol-5-yl)isoquinoline, were synthesized, fully characterized and tested as phosphors for colourless LSCs. Notably, increasing quantities (0.2 – 1.8 w.t. %) of the new Ir(III) based phosphors were dispersed in different acrylate polymers like poly(methyl methacrylate), PMMA, poly(benzyl methacrylate), PBzMA and poly(cyclohexyl methacrylate), PCHMA, leading to visible transparent polymeric films exhibiting excellent photostability and bright yellow to orange phosphorescent emissions. The performances as solar collectors of all the Ir(III)-doped polymers were investigated, providing results comparable, or superior, to those obtained from colourless LSC based on organic fluorophores. In fact, the best optical efficiency (η_{opt} up to 7%, combined to transmittance close to 80% at 390 nm) was displayed by the polymer film obtained from physical dispersion of **[Ir(ppy)$_2$(iQTZ-PPG)]$^+$** (1.4 wt. %) in PCHMA.

Keywords: Ir(III) Cyclometalated Complexes, Tetrazole ligands, Phosphorescent Metal complexes, Luminescent Solar Concentrators, Stokes-Shifts, Transparent polymers, Colourless LSCs.

Introduction

The picture that is usually drawn to describe luminescent Iridium (III) cyclometalated complexes includes a number of recurring expressions such as chemical stability, extreme tuneability of the

redox and excited states properties combined with pronounced Stokes Shifts of the phosphorescent emissions.[1a-b] Taken together, these features showcase most of the reasons that have driven Ir(III) cyclometalates to an outstanding scientific success in all the research areas that rely upon the interaction of light with matter. Beyond to be used as emissive materials for OLED and LEEC -type electroluminescent devices for solid state lighting,[2] which is their "core business" application, luminescent Ir(III) cyclometalated complexes have been exploited in bioimaging and biosensing [3a-b] and, as some of the most recent and important developments, in photoredox catalysis for visible light activated organic reactions [4a-b] and polymerization processes.[5a-b] The opportunity to transfer the excited state properties of discrete Ir(III) complexes to polymeric bulk materials led to various examples of luminescent hybrid macromolecules containing Ir(III)-based fragments as comonomer (metallapolymer) as well as side chain groups.[6] In all cases, the incorporation of Ir(III) complexes within the polymeric backbone has been demonstrated as a promising perspective for improving the luminescent performances of the whole material, since the phosphorescent emitters are most often protected from collisional quenching with dioxygen.[7] In addition, the introduction of such kind of heavy metal complexes entails the possibility of harvesting both singlet and triplet excitons, while the use of organic luminophores would involve only emission from singlet excited states. Taken together, these latter features are not only important for the development of phosphorescent polymer light-emitting diodes (PhPLEDs),[8] but might be extremely relevant for the design of polymer-based materials such as luminescent solar concentrators (LSCs). Starting from their first appearance in 1982, the technology of LSCs has been actively developed both by the side of academic literature and by the one represented by research patents.[9a-d] The importance of LSCs is particularly evident in the photovoltaic context, where the combination of LSCs with solar cells leads to a significant improvement of the energy production as the consequence of the enhancement of the intensity of the incident light. LSCs indeed consist of appropriate and transparent polymeric matrix in which luminescent dyes capable of absorbing the solar radiation and emitting light at lower wavelengths are homogeneously dispersed. Along with traditional LSCs, in which a dye is most often represented by a red-emitting fluorophore – typically, a highly conjugated organic molecule – colourless LSCs have gained an important role since they can be used as architectural windows for building integrated photovoltaics. Notwithstanding, this exciting approach has provided adequate optical efficiencies with a minor degree of coloured tinting,[10a-b] challenges are still open to compete with traditional visible absorbing LSC.[11] Since luminescent Ir(III) cyclometalated complexes meet most of the requirements needed to envisage their use in

LSCs technology - *i.e.* brightly intense emissions tuneable over the whole range of the visible region, large Stokes shifts and excellent photostability, herein we describe the preparation and the characterization of the first examples of polymeric LSCs doped with Ir(III)-based phosphors. For this specific purpose, by taking advantage of our extensive studies on phosphorescent cyclometalated Ir(III) tetrazole complexes with general formula $[Ir(C^N)_2(N^N)]^+$,[12a-c] we have designed and prepared two new red emitting Ir(III) tetrazole complexes (Scheme 1) differing for the nature of the cyclometalating (C^N) ligand, while maintaining the same N^N tetrazole ancillary ligand. More specifically, the two new Ir(III) compounds, abbreviated as **$[Ir(C^N)_2$(iQTZ-PPG)$]^+$**, where (C^N) = **ppy**, 2 phenylpyridine or **npy** = 2-(naphthalen-2-yl)pyridine and **iQTZ-PPG** = 1-(2-(prop-2-yn-1-yl)-2*H*-tetrazol-5-yl)isoquinoline (Scheme 1), were physically dispersed into different polymers and the performances of the corresponding LSCs materials were investigated, highlighting promising potential for the development of colourless LSCs.

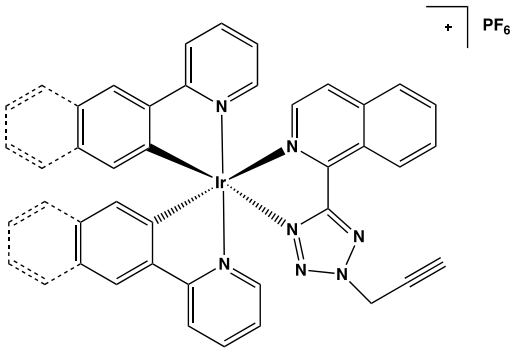

(C^N) = ppy, $[Ir(ppy)_2$(iQTZ-PPG)$]^+$

(C^N) = npy, $[Ir(npy)_2$(iQTZ-PPG)$]^+$

Scheme 1: Ir(III) complexes and relative acronyms employed in this work.

Results and discussions

Synthesis and optical properties in solution

The choice of using cationic Ir(III) tetrazole complexes such as **$[Ir(ppy)_2$(iQTZ-PPG)$]^+$** and **$[Ir(npy)_2$(iQTZ-PPG)$]^+$** (Scheme 1) is explained in consideration of obtaining well soluble phosphors capable of providing red colored emission, a desirable requirement for the organic and lanthanoid-based emitters employed in the LSC technology.[9a-d], [13] Indeed, we have demonstrated how the decoration of the coordinated tetrazolato ring with various alkyl groups is a key factor to determine the consistent shift to lower energy of the emissions of the parent Ir(III)-tetrazolato complexes. In addition, the introduction of a pendant propargyl moiety (PPG), instead of the alkyl residues that we have considered so far was done to pave the way to further functionalization of the Ir(III)

complexes, possibly resulting in their chemical anchoring to monomers [6] or to other organic chromophores.

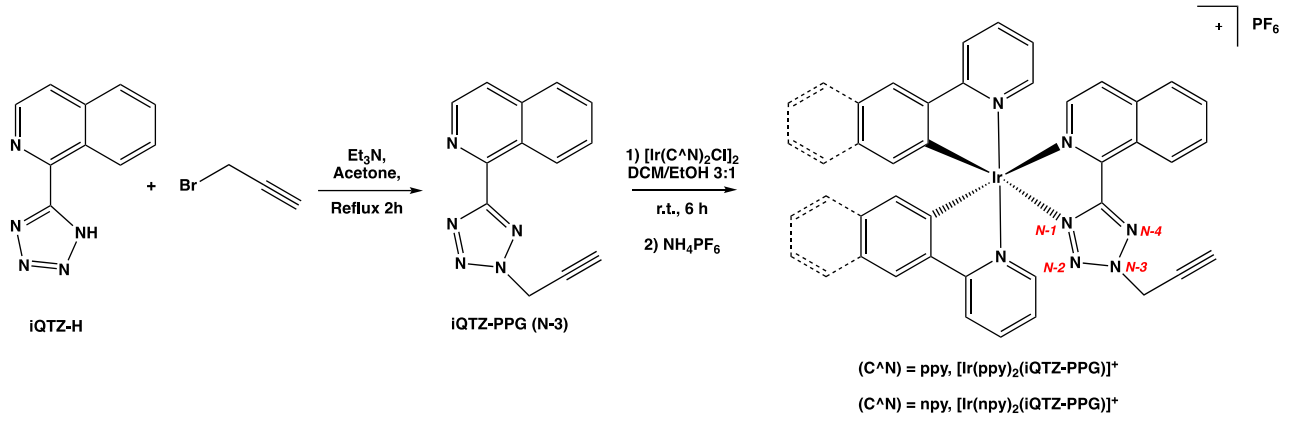

Scheme 2: Synthetic protocol used for the preparation of Ir(III)-tetrazole based complexes with relative acronyms and numeration of the tetrazole ring adopted in this work.

As depicted in Scheme 2, the synthetic strategy to the preparation of the Ir(III) complexes involved the preliminary formation of the tetrazole ligand **iQTZ-PPG**, which was accomplished by functionalization of the isoquinolyl tetrazole molecular scaffold (**iQTZ**) with a propargyl moiety (PPG). As previously observed for electrophilic additions on 5-aryl tetrazoles and related complexes, [12a-c], [14a-e], [15] the reaction of 1-(*1H*-tetrazol-5-yl)isoquinoline (iQTZ-H) with a slight excess of propargyl bromide (Scheme 2), led to the formation of the propargyl appended tetrazole **iQTZ-PPG** as a mixture of N-3 and N-4 substituted regioisomers (see Scheme 2 for atom numbering).[14d] The steric hindrance exerted by the appended PPG group allows for an efficient chelate coordination only in the case of the N-3 regioisomer, in which both isoquinoline and substituted tetrazole rings can adopt the coplanar geometry that is essential to provide a stable chelate -type coordination to the Ir(III) metal ion. Once the the undesired N-4 regioisomer was removed from the crude mixture of regioisomers, the reaction of **iQTZ-PPG** (N-3) with the appropriate dichloro-bridged iridium dimer $[Ir(ppy)_2\text{-}\mu\text{-}Cl]_2$ or $[Ir(npy)_2\text{-}\mu\text{-}Cl]_2$, provided the target complexes **$[Ir(ppy)_2(iQTZ\text{-}PPG)]^+$** and **$[Ir(npy)_2(iQTZ\text{-}PPG)]^+$** (Scheme 2). The identity of each compound was deduced at first by Electron Spray Ionization Mass Spectroscopy (ESI-MS), which returned *m/z* signals compatible with the occurrence of the expected cationic complexes under the form of the corresponding hexafluorophosphate (PF_6^-) salts (Figures S9, S10). The NMR characterization (^1H and ^{13}C, Figures S5 – S8) of the new Ir(III) species provided results congruent with previously reported Ir(III)-tetrazole based complexes with the same C_1 symmetry,[12a-c], [14a-d]. In addition, the chelate coordination of **iQTZ-PPG** as the N-3 regioisomer to the Ir(III) metal centre, was suggested by the typically

downfield-shifted tetrazole carbon resonance (δ C_t), found in all cases at *ca.* 168 ppm (Figures S5, S7). [12a-c], [14a-d]

Photophysical and Theoretical Characterizations

Table 1: Photophysical Data Summary

Complex	**Absorption**	**Emission 298 K[a, b]**					**Emission 77 K[c]**	
CH_2Cl_2 as the solvent 10^{-5}M	λ(nm) 10^{-4}ε ($cm^{-1}M^{-1}$)	λ_{em} (nm)	τ_{ox} (μs)	τ_{deox} (μs)	Φ_{ox} (%)	Φ_{deox} (%)	λ_{em} (nm)	τ (μs)
$[Ir(ppy)_2(iQTZ\text{-}PPG)]^+$	249 (3.94), 300 (1.55), 366 (0.82) 402 (0.51)	650	0.19	0.32	4.0	12.0	544, 590, 640	5.16
$[Ir(npy)_2(iQTZ\text{-}PPG)]^+$	236 (4.21), 275 (3.35), 349 (0.42) 395 (0.23)	636	0.20	0.71	1.0	5.0	548, 592	1.05

[a]: "ox" means air equilibrated solutions, "deox" means deoxygenated solutions under argon atmosphere; [b]: $[Ru(bpy)_3]Cl_2/H_2O$ was used as reference for quantum yield determinations (Φ_r = 0.028)[16]; [c] :in frozen CH_2Cl_2.

The absorption spectra of **$[Ir(ppy)_2(iQTZ\text{-}PPG)]^+$** and **$[Ir(npy)_2(iQTZ\text{-}PPG)]^+$** were obtained from the corresponding diluted (10^{-5} M) CH_2Cl_2 solutions at room temperature. For both Ir(III) complexes (Table 1, Figure 1, left, Figure S11) the absorption profiles typically consisted of intense ligand centred (LC) transitions in the UV region, followed by weaker absorption features tailing beyond 400 nm. In agreement with our previous reports dealing with Ir(III) tetrazolato and Ir(III)-tetrazole complexes, [12a-c], [14a-d] these latter transitions were assigned to the occurrence of ligand-to-ligand charge transfer (LLCT) and metal-to-ligand charge transfer (MLCT) processes.

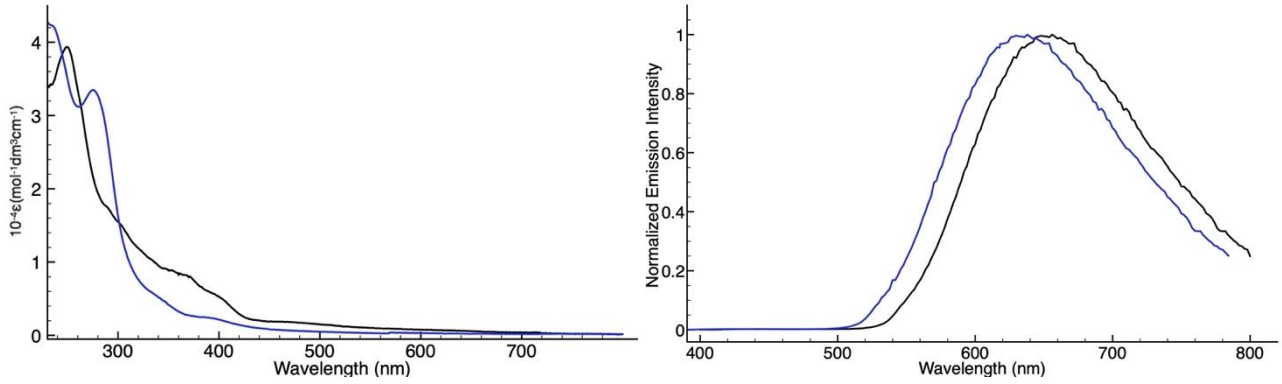

Figure 1: (left) Absorption profiles of **$[Ir(ppy)_2(iQTZ\text{-}PPG)]^+$** (black trace) and **$[Ir(npy)_2(iQTZ\text{-}PPG)]^+$** (blue trace), 10^{-5}M, CH_2Cl_2, 298K; (right) Normalized emission profiles of **$[Ir(ppy)_2(iQTZ\text{-}PPG)]^+$** (black trace) and **$[Ir(npy)_2(iQTZ\text{-}PPG)]^+$** (blue trace), CH_2Cl_2, 298K.

Upon photoexcitation (λ_{exc} = 350 nm) of the corresponding diluted solutions at 298K, **$[Ir(ppy)_2(iQTZ\text{-}PPG)]^+$** and **$[Ir(npy)_2(iQTZ\text{-}PPG)]^+$** displayed red emissions peaking at λ_{max} = 630 and 650 nm respectively (Figure 2, Figures S12, S15). In both cases, the broad and structureless shape of the

emission profiles suggested the prevalent charge transfer (CT) nature of the emissive excited states. Further in support to this assignment was the pronounced *rigidochromic* blue shift displayed by each of the emission profiles upon passing from 298 to 77K (Figures S14, S17). The emissions stemming from both **[Ir(ppy)$_2$(iQTZ-PPG)]$^+$** and **[Ir(npy)$_2$(iQTZ-PPG)]$^+$** displayed marked sensitivity to dissolved dioxygen. Indeed, upon degassing, the solutions of the Ir(III) complexes in CH_2Cl_2 showed increased quantum yield (Φ), with a concomitant elongation of the excited states lifetimes (τ, Table 1). therefore suggesting the triplet multiplicity of the emissive excited states. Taken together, these features are consistent with the minimum energy geometries and the electronic structures of **[Ir(ppy)$_2$(iQTZ-PPG)]$^+$** and **[Ir(npy)$_2$(iQTZ-PPG)]$^+$**, which were characterized by the means of DFT and TD-DFT calculations including the effect of the solvent medium (*i.e.* CH_2Cl_2). In regards of the ground electronic state of the Ir(III) complexes, both systems displayed HOMO levels mainly centred on the transition metal, with relevant contributions from the cyclometalated ligands **ppy** and **npy**. On the contrary, in excellent agreement with our previous reports dealing with similar cationic Ir(III) tetrazole complexes,[12a], [14c,d] the LUMO levels are prevalently localized on whole π-conjugated system of the tetrazole ligand **(iQTZ-PPG)**, without any contribution of the cyclometalated ligands.(Figure 2).

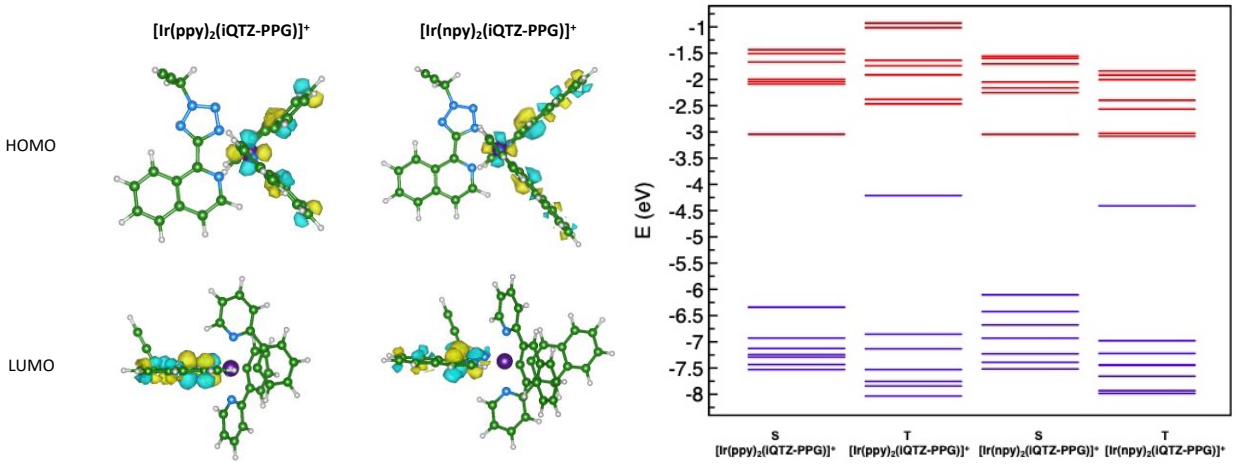

Figure 2: (left) Minimum-energy geometries and isodensity surface plots of the HOMO and LUMO of **Ir(ppy)$_2$(iQTZ-PPG)]$^+$** and **[Ir(npy)$_2$(iQTZ-PPG)]$^+$** (contour value set to 0.005 au). Colour legend: green for C atoms, blue for N atoms, purple for Ir atoms and white for H atoms; isodensity positive and negative values are in yellow and cyan, respectively; (right) Energy level diagram from HOMO-6 to LUMO+6 for both singlet (S) and triplet (T) optimized geometries of **Ir(ppy)$_2$(iQTZ-PPG)]$^+$** and **[Ir(npy)$_2$(iQTZ-PPG)]$^+$**: occupied orbital (blue), unoccupied orbital (red).

The vertical excitation energies for the spin-allowed electronic transitions are listed in Table 2. According to the experimental data, the intense high-energy absorption bands are composed of LC transitions, with λ_{cal} = 302/335 and 324/332 nm for **[Ir(ppy)$_2$(iQTZ-PPG)]$^+$** and **[Ir(npy)$_2$(iQTZ-PPG)]$^+$**,

respectively. Instead, the weak lower energy bands beyond 400 nm can be assigned to MLCT and LLCT transitions. In the case of **[Ir(npy)$_2$(iQTZ-PPG)]$^+$**, the LC transitions mostly involve the **(npy)** ligands, whereas in **[Ir(ppy)$_2$(iQTZ-PPG)]$^+$** both **(ppy)** and **(iQTZ-PPG)** are involved. Moreover, the two Ir(III) complexes were optimized in the triplet state, which is speculated to be the final excited electronic state from which the emission occurs. The comparison between singlet and triplet optimized geometries displayed no significant structural variations, with only one of the two cyclometalated ligands (**ppy** or **npy)** coming closest to the chelate tetrazole ligand **(iQTZ-PPG)**, where the triplet state is mostly localized (consistently with the positions of the singlet's LUMOs). The computed vertical emission have returned transition located in the red region at λ_{em} = 574 and 616 nm for **[Ir(ppy)$_2$(iQTZ-PPG)]$^+$** and **[Ir(npy)$_2$(iQTZ-PPG)]$^+$**, respectively, and could be therefore ascribed to MLCT-LLCT spin-forbidden transitions, as observed experimentally.

Table 2: TD-DFT calculated lowest excited singlet states and character of the transitions for the two complexes [PBE0/SDD/6-31G++(d,p)/PCM=CH_2Cl_2].

Complex	ΔE_{cal} (eV) [a]	λ_{cal} (nm) [b]	f [c]	Electronic transition assignment [d]	Nature of the transition
[Ir(ppy)$_2$(iQTZ-PPG)]$^+$	4.11	302	0.077	HOMO-1 → LUMO+3 (54%) HOMO-2 → LUMO+2 (24%)	LC
	3.70	335	0.128	HOMO-6 → LUMO (68%)	LC
	3.45	359	0.078	HOMO → LUMO+2 (41%) HOMO-3 → LUMO (37%)	MLCT + LLCT
	3.31	374	0.072	HOMO → LUMO+1 (66%)	MLCT + LC
	2.50	496	0.001	HOMO → LUMO (70%)	MLCT + LLCT
[Ir(npy)$_2$(iQTZ-PPG)]$^+$	3.83	324	0.208	HOMO-2 → LUMO+2 (46%) HOMO → LUMO+6 (43%)	LC + MLCT
	3.73	332	0.341	HOMO-2 → LUMO+1 (59%) HOMO → LUMO+4 (27%)	LC + MLCT
	3.49	354	0.191	HOMO-1 → LUMO+1 (50%) HOMO-5 → LUMO (44%)	LC + MLCT
	3.04	407	0.040	HOMO→ LUMO+1 (68%)	LC + MLCT
	2.35	526	0.0002	HOMO → LUMO (69%)	MLCT + LLCT

[a]: ΔE_{calc} is the main transition energy; [b]: λ_{calc} is the calculated λ_{max}; [c]: f is the oscillator strength; [d]: Main Kohn–Sham orbital contribution to the electronic transition.

Preparation and optical properties of LSCs

In order to assess their potential as phosphorescent dopants for colourless LSCs, increasing quantities (0.2 – 1.8 wt. %) of the Ir(III)-based phosphors **[Ir(ppy)$_2$(iQTZ-PPG)]$^+$** and **[Ir(npy)$_2$(iQTZ-PPG)]$^+$** were physically dispersed into different acrylate polymers. In particular, aside to the "conventional" poly(methyl methacrylate) (PMMA, Mw = 350,000 g/mol, T_g = 105 °C), other amorphous and visibly transparent polymer matrices such as poly(benzyl methacrylate) (PBzMA, Mw = 100,000 g/mol, T_g = 54 °C) and poly(cyclohexyl methacrylate) (PCHMA, Mw = 65,000 g/mol, T_g = 104 °C), were considered. The obtained polymeric films were initially screened for their homogeneity and transparency. In this regard, both complexes **[Ir(ppy)$_2$(iQTZ-PPG)]$^+$** and **[Ir(npy)$_2$(iQTZ-PPG)]$^+$** were found to be compatible with PMMA within the range of the investigated concentrations (0.2 – 1.8 wt. %) and optically very similar under ambient and UV light excitation. As an example, pictures of PMMA polymer films containing from 0.2 to 1.8 wt.% of **[Ir(npy)$_2$(iQTZ-PPG)]$^+$** deposited onto Edmund 50x50x3 mm glass are reported in Figure 3.

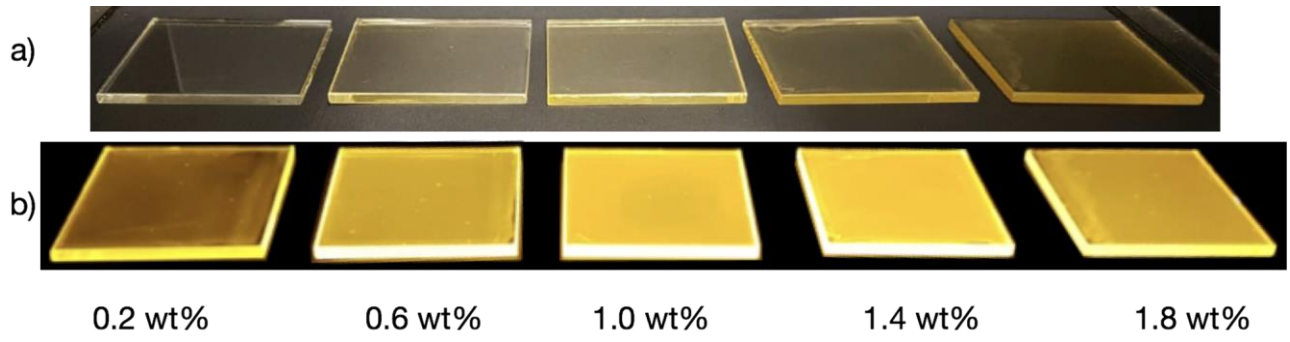

Figure 3. Left to right: PMMA polymer films containing from 0.2 to 1.8 wt. %of **[Ir(npy)$_2$(iQTZ-PPG)]$^+$** deposited onto Edmund 50x50x3 mm glass irradiated with a) under ambient light and b) under near UV lamp (λ_{max} 366 nm).

Conversely, transparent and homogeneous polymeric films based on PBzMA and PCHMA were obtained from **[Ir(ppy)$_2$(iQTZ-PPG)]$^+$** only, being **[Ir(npy)$_2$(iQTZ-PPG)]$^+$** found to be less compatible with the less polar PBzMA and PCHMA matrices (Figure S18). Epifluorescence microscopy images displayed the distribution within the PMMA matrix of very small **[Ir(ppy)$_2$(iQTZ-PPG)]$^+$** aggregates that downsized to almost molecular level when embedded into highly compatible less polar PBzMA and PCHMA matrices (Figure 4).[17a-b]

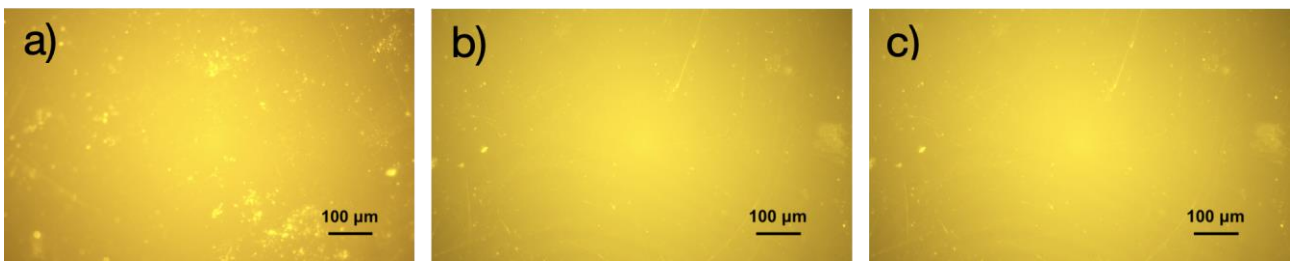

Figure 4. Epifluorescence images of 1.4 wt. % **[Ir(ppy)$_2$(iQTZ-PPG)]$^+$** doped a) PMMA, b) PBzMA and c) PCHMA polymer films (λ_{exc} 365 nm). Scale bar = 100 µm.

The transparent and colourless appearance of all the Ir(III) doped polymer films was correlated with the lack of any appreciably intense transition in the visible region of the corresponding absorption spectra, with transmittance values close to 80% for the films containing 1.4 wt. % of fluorophore doping (Figure S19). Indeed, the absorption profiles of the Ir(III) complexes dispersed within the various polymer matrices and deposited onto optically pure 50 X 50 X 3 mm Edmund glass (Figure 5A and 5C) were found to be very similar to those obtained from the corresponding dichloromethane solutions, with intense ligand centred (LC) transitions peaking in the UV region and weaker CT processes centred at lower energy and marginally tailing off the visible region. In addition, the intensity of the various transitions was found to vary according to the different contents of the Ir(III) complexes in the polymeric films.

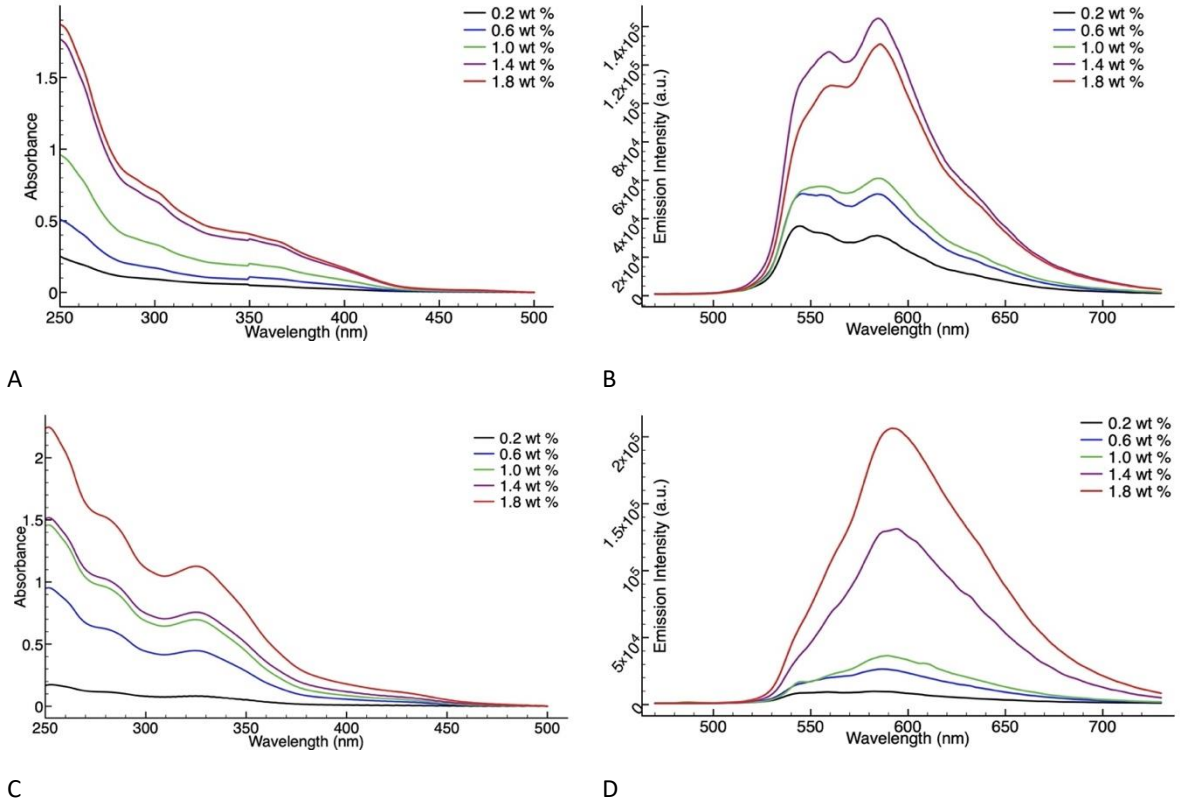

Figure 5. Absorption and emission (λ_{exc} = 350 nm) profiles of PMMA films containing different amounts of **[Ir(ppy)$_2$(iQTZ-PPG)]$^+$** (A, B), and **[Ir(npy)$_2$(iQTZ-PPG)]$^+$**, (C, D).

Upon excitation at λ = 350 nm, all the Ir(III) doped polymer matrices displayed bright yellow luminescence (see Figures 3 and 4), suggesting the occurrence of a very pronounced Stokes Shift for both the Ir(III)- based species (Figure 5, Table 3). If compared to what observed for the corresponding liquid solutions at room temperature, the Ir(III) complexes dispersed in the polymer

matrices displayed significantly blue shifted and structured emission profiles. This behaviour can be traced back to the prevalent CT nature of the emissive excited states and to the interplay of ^{3}MLCT and ^{3}LLCT contributions in their composition. Such admixture is likely responsible for the appearance of vibronic progressions in the emission profiles of all the polymer matrices containing **[Ir(ppy)$_2$(iQTZ-PPG)]$^+$** and **[Ir(npy)$_2$(iQTZ-PPG)]$^+$** (Figures 5 and 6).

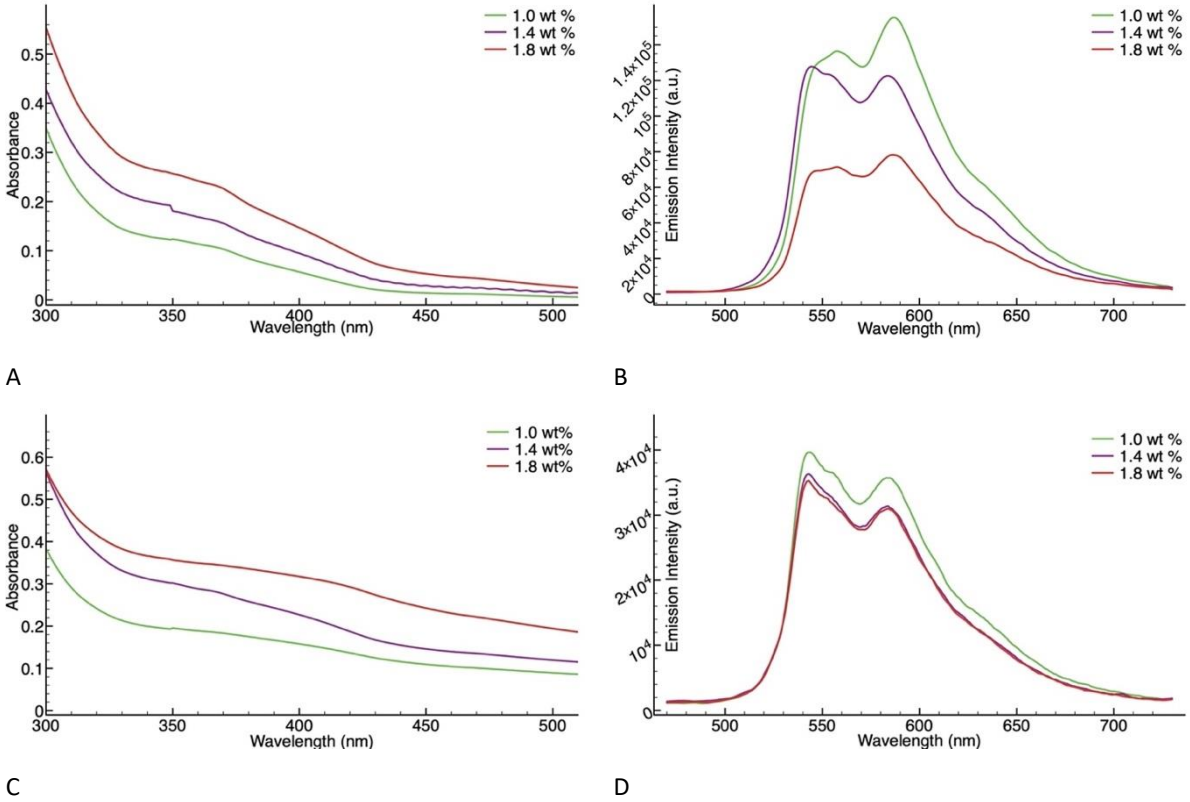

Figure 6. Absorption and emission (λ_{exc} = 350 nm) profiles of **[Ir(ppy)$_2$(iQTZ-PPG)]$^+$** dispersed into PBzMA (A, B), and PCHMA, (C, D).

With the sole exception of **[Ir(npy)$_2$(iQTZ-PPG)]$^+$** (Figure 5, C-D), a decrease in the emission intensity of the polymer matrices was observed upon increasing complex doping (Figure 5 A-B, Figure 6). This trend might be explained in consideration of the occurrence of auto-quenching or aggregation-induced quenching phenomena at high Ir(III) complex doping and to the partial overlap of absorption and emission features of **[Ir(ppy)$_2$(iQTZ-PPG)]$^+$**. Relative to the analysis of the absolute quantum yields (Φ) of the Ir(III)-complexes dispersed in the various polymers (Figure 7 and Table 3), the results obtained from the PMMA matrices showed the highest Φ values, *i.e.*, 41% for **[Ir(ppy)$_2$(iQTZ-PPG)]$^+$** and 28% for **[Ir(npy)$_2$(iQTZ-PPG)]$^+$** for the samples containing the lowest content (0.2 wt. %) of Ir(III) complex, while progressive decrease of Φ took place upon enhancing their concentration.

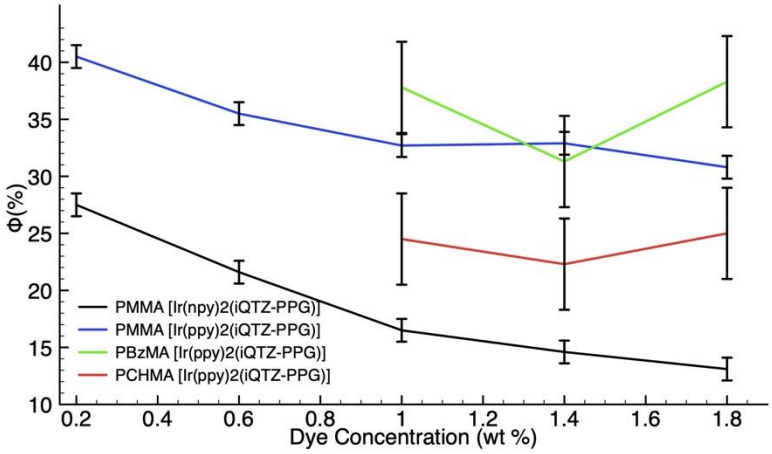

Figure 7. Quantum yield (Φ) trends for the different contents of **[Ir(ppy)$_2$(iQTZ-PPG)]$^+$** and **[Ir(npy)$_2$(iQTZ-PPG)]$^+$** dispersed into PMMA, PBzMA, and PCHMA.

Different trends were observed for the quantum yield (Φ) of **[Ir(ppy)$_2$(iQTZ-PPG)]$^+$** in PBzMA and PCHMA, where the highest values were displayed by the polymer matrices containing 1.0 wt. % and 1.8 wt. %, with lower values being displayed by the intermediate concentration (1.4 wt. %) although almost comprised within the experimental error. Among the PBzMA and PCHMA polymers, in which the higher and ideal contents for LSC application of **[Ir(ppy)$_2$(iQTZ-PPG)]$^+$** are dispersed, the remarkably better Φ values was displayed by the PBzMA matrices containing 1.0 wt. % of the Ir(III) complex **[Ir(ppy)$_2$(iQTZ-PPG)]$^+$**. Notably, the better phase dispersion of **[Ir(ppy)$_2$(iQTZ-PPG)]$^+$** in PBzMA and PCHMA (Figure 4) resulted helpful in gathering the highest quantum efficiencies for the former system only, possibly due to the beneficial effect provided by the aromatic moieties in maximizing the polymer/fluorophore interaction thus limiting the adverse effect due to aggregation. Photostability of **[Ir(ppy)$_2$(iQTZ-PPG)]$^+$** and **[Ir(npy)$_2$(iQTZ-PPG)]$^+$** embedded into PMMA were also investigated by continuously irradiating a 0.25 cm^2 spot of the PMMA films at 350 nm with a 450 W Xe arc lamp under aerobic conditions. It is noteworthy that both **[Ir(ppy)$_2$(iQTZ-PPG)]$^+$** and **[Ir(npy)$_2$(iQTZ-PPG)]$^+$** almost retained their emission after two hours of continuous excitation (Figure S20), thus suggesting excellent photostability.

Before passing on studying the performances of the derived LSCs, the absorption and emission profiles of the **[Ir(ppy)$_2$(iQTZ-PPG)]$^+$** and **[Ir(npy)$_2$(iQTZ-PPG)]$^+$** embedded into polymer matrices were compared to the solar spectrum and the external quantum efficiency (EQE) of the utilized Si PV cell (Figure 8). Notably, the absorption tails between 380 and 450 nm allowed to capture the near-UV solar window, whereas the emission exactly matches the highest EQE values of the Si PV cell, thus suggesting the optimal conversion of re-emitted photons into electrical current. It is worth

noting the large Stokes shift (Table 3) displayed by the Ir(III) complexes in PMMA, a feature that is considered beneficial in limiting efficiency losses in LSCs. [9a]

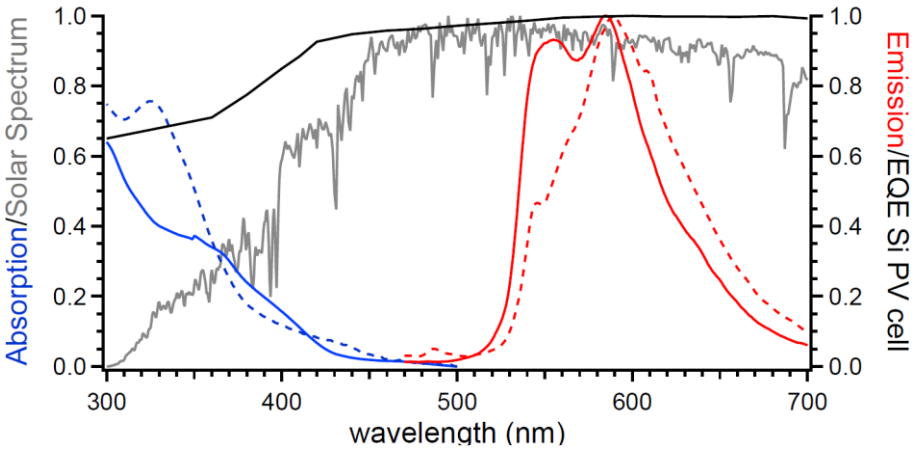

Figure 8. Absorption (blue continuous line for **[Ir(ppy)$_2$(iQTZ-PPG)]$^+$** and dashed line for **[Ir(npy)$_2$(iQTZ-PPG)]$^+$**) and normalized emission (λ_{exc} = 350 nm, red continuous line for **[Ir(ppy)$_2$(iQTZ-PPG)]$^+$** and dashed line for **[Ir(npy)$_2$(iQTZ-PPG)]$^+$**) spectra of 1.4 wt. % Ir(III) complexes in PMMA. The solar spectral irradiance at air mass 1.5 (AM 1.5) collected from American Society for Testing and Materials (ASTM) is reported in gray.[18] The black line represents the EQE curve of the Si PV cell used in this work.

Furthering these premises, the performances as solar collectors of all the PMMA, PBzMA and PCHMA-based films containing the various amounts of the Ir(II) complexes **[Ir(ppy)$_2$(iQTZ-PPG)]$^+$** and **[Ir(npy)$_2$(iQTZ-PPG)]$^+$** were determined on optically pure 50 X 50 X 3 mm Edmund glass by using a Si-based PV cell attached to one edge of the LSC. The power obtained from the PV cell was measured combined with the LSC (P_{LSC}) and directly exposed to a AM 1.5 solar simulator (P_{LC}). The optical efficiency (η_{opt}) was then calculated according to equation 2 (*Experimental Section*) with geometric factor (G), which is the ratio between the area exposed to the light source and the collecting area, corresponding to 16.6 in our case (Figure 8 and Table 4).

Table 3: LSC's photophysical data summary.

Polymer/Ir(III) complex/wt. %	Absorption	Emission		
	λ (nm)	λ (nm)	Φ (%)	Stokes Shift (cm^{-1})
PMMA $[Ir(npy)_2(iQTZ\text{-}PPG)]^+$ 0.2 %	285	543, 585	27.5±1	16671
PMMA $[Ir(npy)_2(iQTZ\text{-}PPG)]^+$ 0.6 %	285, 302	543, 585	21.6±1	14696
PMMA $[Ir(npy)_2(iQTZ\text{-}PPG)]^+$ 1.0 %	289, 302, 368	549, 585	16.5±1	8959
PMMA $[Ir(npy)_2(iQTZ\text{-}PPG)]^+$ 1.4 %	289, 300, 368	560, 585	14.6±1	9316
PMMA $[Ir(npy)_2(iQTZ\text{-}PPG)]^+$ 1.8 %	302, 352, 368	558, 585	13.1±1	9252
PMMA $[Ir(ppy)_2(iQTZ\text{-}PPG)]^+$ 0.2 %	284, 325	588	40.5±1	13763
PMMA $[Ir(ppy)_2(iQTZ\text{-}PPG)]^+$ 0.6 %	284, 325	587	35.5±1	13734
PMMA $[Ir(ppy)_2(iQTZ\text{-}PPG)]^+$ 1.0 %	284, 325	588	32.7±1	13763
PMMA $[Ir(ppy)_2(iQTZ\text{-}PPG)]^+$ 1.4 %	284, 325	592	32.9±1	13878
PMMA $[Ir(ppy)_2(iQTZ\text{-}PPG)]^+$ 1.8 %	284, 325	593	30.8±1	13906
PBzMA $[Ir(ppy)_2(iQTZ\text{-}PPG)]^+$ 1.0 %	370	544, 585	37.8±4	8645
PBzMA $[Ir(ppy)_2(iQTZ\text{-}PPG)]^+$ 1.4 %	370	548, 586	31.3±4	8779
PBzMA $[Ir(ppy)_2(iQTZ\text{-}PPG)]^+$ 1.8 %	370	546, 586	38.3±4	8712
PCHMA $[Ir(ppy)_2(iQTZ\text{-}PPG)]^+$ 1.0 %	380	542, 584	24.2±4	8765
PCHMA $[Ir(ppy)_2(iQTZ\text{-}PPG)]^+$ 1.4 %	380	542, 584	22.3±4	8765
PCHMA $[Ir(ppy)_2(iQTZ\text{-}PPG)]^+$ 1.8 %	380	542, 584	25.0±4	8765

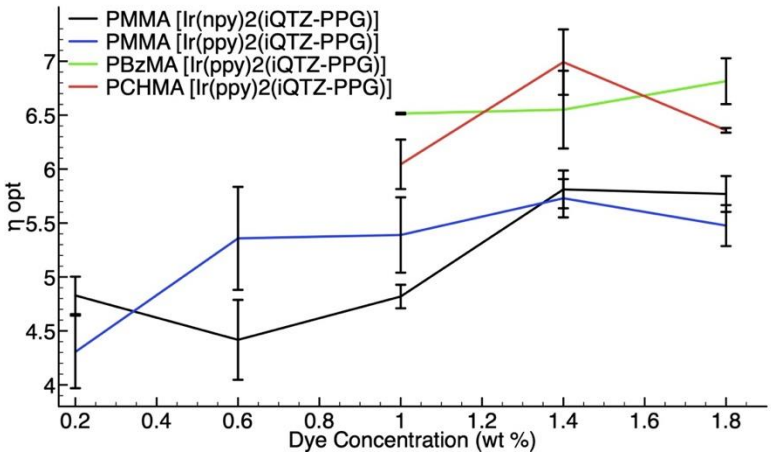

Figure 9. Optical efficiencies of the different contents of **$[Ir(ppy)_2(iQTZ\text{-}PPG)]^+$** and **$[Ir(npy)_2(iQTZ\text{-}PPG)]^+$** dispersed into PMMA, PBzMA, and PCHMA.

In particular, the η_{opt} values appeared to increase along with fluorophores contents thanks to the solar harvesting provided by the dispersed amount of absorbing chromophores, although adversely

affected by emission dissipative phenomenon that caused their levelling-off at doping contents higher than 1.4 wt. % and reaching maximum values of about 6%. Notably, in case of PMMA dispersions, the higher Φ and Stokes Shift of **[Ir(ppy)$_2$(iQTZ-PPG)]$^+$** than that of **[Ir(npy)$_2$(iQTZ-PPG)]$^+$** contributed in greater η_{opt} for fluorophore content lower than 1.4 wt. %, only. This unexpected phenomenon could be possibly addressed to the presence of the additional absorption band at 368 nm for the **[Ir(npy)$_2$(iQTZ-PPG)]$^+$** fluorophore that made a greater contribution in solar harvesting at high doping contents. Anyway, η_{opt} of about 6% means a concentration factor close to 1, (G=16.6), *i.e.* higher than those of transparent thin-film LSCs based on Tb^{3+} and Eu^{3+} emitters [19] although still lower than those with organic dopants.[20]

Table 4. Optical efficiencies (η_{opt}) for the LSCs based on the Ir(III) complexes dispersed in the various polymer matrices

Polymer/Ir(III) complex/wt. %	η_{opt} (%)
PMMA [Ir(npy)$_2$(iQTZ-PPG)]$^+$ 0.2 %	4.8 ± 0.17
PMMA [Ir(npy)$_2$(iQTZ-PPG)]$^+$ 0.6 %	4.4 ± 0.37
PMMA [Ir(npy)$_2$(iQTZ-PPG)]$^+$ 1.0 %	4.8 ± 0.11
PMMA [Ir(npy)$_2$(iQTZ-PPG)]$^+$ 1.4 %	5.8 ± 0.17
PMMA [Ir(npy)$_2$(iQTZ-PPG)]$^+$ 1.8 %	5.8 ± 0.17
PMMA [Ir(ppy)$_2$(iQTZ-PPG)]$^+$ 0.2 %	4.3 ± 0.34
PMMA [Ir(ppy)$_2$(iQTZ-PPG)]$^+$ 0.6 %	5.4 ± 0.48
PMMA [Ir(ppy)$_2$(iQTZ-PPG)]$^+$ 1.0 %	5.4 ± 0.35
PMMA [Ir(ppy)$_2$(iQTZ-PPG)]$^+$ 1.4 %	5.7 ± 0.18
PMMA [Ir(ppy)$_2$(iQTZ-PPG)]$^+$ 1.8 %	5.5 ± 0.19
PBzMA [Ir(ppy)$_2$(iQTZ-PPG)]$^+$ 1.0 %	6.5 ± 0.01
PBzMA [Ir(ppy)$_2$(iQTZ-PPG)]$^+$ 1.4 %	6.6 ± 0.36
PBzMA [Ir(ppy)$_2$(iQTZ-PPG)]$^+$ 1.8 %	6.8 ± 0.21
PCHMA [Ir(ppy)$_2$(iQTZ-PPG)]$^+$ 1.0 %	6.0 ± 0.23
PCHMA [Ir(ppy)$_2$(iQTZ-PPG)]$^+$ 1.4 %	7.0 ± 0.30
PCHMA [Ir(ppy)$_2$(iQTZ-PPG)]$^+$ 1.8 %	6.4 ± 0.02

Nevertheless, the beneficial effect of the phase compatibility provided by PBzMA and PCHMA matrices was particularly reflected on the LSC performances. Notably, as reported in Table 4, the 1.4 wt. % of **[Ir(ppy)$_2$(iQTZ-PPG)]$^+$** dispersed into PCHMA provided the highest η_{opt} of 7%, that is comparable, if not superior, to the LSC efficiencies recently obtained by using visible transparent

organic fluorophores such as bis[1-(thiophenyl)propynones] and bis azole derivatives.[10a-b] Very similar η_{opt} of 6.8% was reached by the same phosphor dispersed into PBzMA at the highest 1.8 wt. % content, thanks to the beneficial effect provided by the higher Φ of 38%. Notably, the reduction of the Stokes shift that occurred on passing to polymer matrices with less polar character did not adversely affected the LSC efficiencies, possibly due to a more pronounced maximum absorption in the visible region (*i.e.* 370-380 nm against 325 nm) that again contributed in larger solar harvesting features. Overall, the performances reached by using the Ir(III) based phosphors are considered worthwhile since obtained by large Stokes shift fluorophores that provided to the LSC transmittance close to 80% at 390 nm. This features also suggest their use in combination with NIR absorbing organic fluorophores, as effectively reported in a recent literature.[21] The dual-band selective-harvesting LSC would boost the power generation while maintaining intact the aesthetic features of the device.

Conclusions

In conclusion, we have shown the first real example of Luminescent Solar Concentrators (LSCs) based on phosphorescent Ir(III) cyclometalated complexes. More precisely, our strategy involved the simple physical dispersion – instead of the synthetically more difficult chemical anchoring - of variable amounts of two new and appositely designed Ir(III) complexes into different acrylate polymers - such as PMMA, PBzMA, or PCHMA - leading to the obtainment of visible-transparent and highly photostable polymer films. These films displayed a very good potential as colourless LSCs, as witnessed by the PCHMA film doped with **$[Ir(ppy)_2(iQTZ\text{-}PPG)]^+$** (1.4 wt. %) exhibiting the best optical efficiency (η_{opt} up to 7%) combined to transmittance close to 80% at 390 nm. Beyond to these promising results, our findings might pave the way for the design of “hybrid” LSCs, in which the global performances - both in terms of an extended solar light harvesting and panchromatic emission - might be significantly improved with the synergistic and possibly beneficial effect deriving from the combination of “traditional” organic fluorophores with this kind of Ir(III)-based phosphors. Research efforts aimed at developing these new aspects are currently being pursued in our labs.

Experimental Section

General considerations. All the reagents and solvents were obtained commercially (Sigma Aldrich/Merck, Alfa Aesar, Strem Chemicals) and used as received without any further purification, unless otherwise specified. When required, the reactions were carried out under an argon atmosphere following Schlenk protocols. The purification of the Ir(III) complexes was performed via column chromatography with the use of SiO_2 as the stationary phase. ESI-mass spectra were recorded using a Waters ZQ-4000 instrument (ESI-MS, acetonitrile as the solvent). Nuclear magnetic resonance spectra (consisting of ^{1}H and **^{13}C{^{1}H}**) were always recorded using a Varian Mercury Plus 400 (^{1}H, 399.9; **^{13}C{^{1}H}**, 101.0 MHz). ^{1}H and **^{13}C{^{1}H}** chemical shifts were referenced to residual solvent resonances.

Photophysics of Ir(III) complexes. Absorption spectra were recorded at room temperature using a Cary 100 UV/vis spectrometer, Agilent Technologies. Uncorrected steady-state emission and excitation spectra were recorded on an Edinburgh FLSP920 spectrometer equipped with a 450 W xenon arc lamp, double excitation and single emission monochromators, and a Peltier-cooled Hamamatsu R928P photomultiplier tube (185−850 nm). Emission and excitation spectra were acquired with a cut-off filter and corrected for source intensity (lamp and grating) and emission spectral response (detector and grating) by a calibration curve supplied with the instrument. The wavelengths for the emission and excitation spectra were determined using the absorption maxima of the MLCT transition bands (emission spectra) and at the maxima of the emission bands (excitation spectra). Quantum yields (Φ) were determined using the optically dilute method by Crosby and Demas,[22] at excitation wavelength obtained from absorption spectra on a wavelength scale [nm] and compared to the reference emitter by the following equation:[23]

$$\Phi_s = \Phi_r \left[\frac{A_r}{A_s}\frac{(\lambda_r)}{(\lambda_s)}\right]\left[\frac{I_r}{I_s}\frac{(\lambda_r)}{(\lambda_s)}\right]\left[\frac{n_s^2}{n_r^2}\right]\left[\frac{D_s}{D_r}\right] \quad \text{(Equation 1)}$$

where A is the absorbance at the excitation wavelength (λ), I is the intensity of the excitation light at the excitation wavelength (λ), n is the refractive index of the solvent, D is the integrated intensity of the luminescence, and Φ is the quantum yield. The subscripts r and s refer to the reference and the sample, respectively. A stock solution with an absorbance > 0.1 was prepared, then a 10 times diluted solution was obtained, resulting in absorbance of about 0.07/0.08 depending on the sample considered. The Lambert-Beer law was assumed to remain linear at the concentrations of the solutions. The degassed measurements were obtained after the solutions were bubbled for 10

minutes under Ar atmosphere, using a septa-sealed quartz cell. Air-equilibrated $[Ru(bpy)_3]Cl_2/H_2O$ solution ($\Phi_r = 0.028$) [16] was used as reference. The quantum yield determinations were performed at identical excitation wavelengths for the sample and the reference, therefore deleting the I(λr)/I(λs) term in Equation 1. Emission lifetimes (τ) were determined with the single photon counting technique (TCSPC) with the same Edinburgh FLSP920 spectrometer using pulsed picosecond LED (EPLED 360, FWHM < 800ps) as the excitation source, with repetition rates between 1 kHz and 1 MHz, and the above-mentioned R928P PMT as detector. The goodness of fit was assessed by minimizing the reduced χ2 function and by visual inspection of the weighted residuals. To record the 77 K luminescence spectra, the samples were put in quartz tubes (2 mm diameter) and inserted in a special quartz Dewar filled with liquid nitrogen. The solvent used in the preparation of the solutions for the photophysical investigations was of spectrometric grade. Experimental uncertainties are estimated to be ±8% for lifetime determinations, ±20% for quantum yields, and ±2 nm and ±5 nm for absorption and emission peaks, respectively.

LSC materials and preparation. Poly(methyl methacrylate) (PMMA, Sigma Aldrich, Mw = 350,000 g/mol, T_g = 105 °C), Poly(benzyl methacrylate) (PBzMA, Sigma Aldrich, Mw = 100,000 g/mol, T_g = 54 °C) and Poly(cyclohexyl methacrylate) (PCHMA, Sigma Aldrich, Mw = 65,000 g/mol, T_g = 104 °C) were used as received. PMMA thin films of **$[Ir(ppy)_2(iQTZ\text{-}PPG)]^+$** and **$[Ir(npy)_2(iQTZ\text{-}PPG)]^+$** were prepared by drop-casting, *i.e.* pouring 1.2 mL of a $CHCl_3$ solution containing about 60 mg of the polymer and different concentrations (0.2-1.8 wt. %) of the Ir(III) phosphor on a 50×50×3 mm optically pure glass substrate (Edmund Optics Ltd BOROFLOAT window 50×50 TS). The glass slides were cleaned with chloroform and immersed in 6 M HCl for at least 12 h and in agreement with procedures previously reported.[24], [25a-b], [26a-d] The film thickness was measured by a Starrett micrometer to be 25 ± 5 μm.

LSC Equipment and techniques. UV-vis absorption spectroscopy was performed at room temperature by using an Agilent Cary 5000 spectrophotometer. Emission spectra were measured at room temperature with a Horiba Jobin–Yvon Fluorolog® -3 spectrofluorometer equipped with a 450W Xenon arc lamp and double-grating excitation and single-grating emission monochromators. The absolute quantum yields (Φ) were determined by using a 152 mm diameter "Quanta-ϕ" integrating sphere, coated with Spectralon® and following the procedures recently reported.[10a-b] Epifluorescence micrographs were taken by a LED epifluorescence microscope (Schaefer South-East Europe Srl, Rovigo, Italy) equipped with a LED blue and green 5W epifluorescence illumination and a DeltaPix Invenio 2EIII 160 microscope camera (DeltaPix, Smorum, Denmark). The concentration

factors and the optical efficiencies of the LSC was obtained by using a solar simulator (ORIEL® LCS-100 solar simulator 94011A S/N: 322, AM1.5G std filter: 69 mW/cm^{-2} at 254 mm) and a calibrated PV cell (IXYS SLMD121H08L mono solar cell 86×14 mm) [25a-b], [26a], [27], [28] connected to a precision source/measure unit (Keysight Technologies B2900 Series). The PV cell is masked with black tape to match LSC edge (50 mm x 3 mm) to make stray light negligible. High purity silicon was used to grease the PV cell to the LSC edge to limit flux losses.[26d] Only one edge of the waveguide was attached to the PV cell to make the wiring connections simple. The other three edges of the LSC were covered with a tape in agreement with the recent literature.[29] The optical efficiency η_{opt} was determined from the concentration factor, *i.e.* the ratio between the maximum power measured for the cell over the LSC edge (P_{LSC}) and that of the bare cell when exposed to the light source (P_{SC}):

$$\eta_{opt} = \frac{P_{LSC}}{P_{SC} \cdot G} \qquad \text{(Equation 2)}$$

where G is the geometrical factor (G = 16.66) that is the ratio between the area exposed to the solar simulator and the collecting area by the PV cell. Notably, during the P_{LSC} measurements, a white back scattering layer (ERGA TAPES Srl Microcellular MCPET reflective sheet) was placed beneath the LSC with an air gap of about 5 mm. The reported η_{opt} values were calculated as the average of three distinct.

Computational Details. All of the theoretical calculations were carried out with the Gaussian16 program.[30] The optimization of the geometries for both singlet ground-state and first triplet-excited state was carried out by using the DFT method at the PBE0[31] level of theory with the]Becke-Johnson damped version of Grimme's dispersion D3 (D3-BJ).[32] We employed the SDD effective core potential and basis sets[33] for Ir and the 6-31++G(d,p) basis set[34] for N, C and H atoms. Such approach has been recently validated for similar Ir(III) complexes.[35] The absence of negative frequencies in the vibrational analysis was used as a parameter to confirm the reliability of the optimized geometries. Vertical excitation energies have been computed by using the time-dependent DFT (TD-DFT) with the optimized singlet ground-state geometries. In all calculations, we took into account the solvent medium by means of the polarizable continuum model (PCM) of implicit solvation[36] with default parameters for dichloromethane (CH_2Cl_2), as implemented in Gaussian16.

Ligand synthesis. Tetrazole derivatives can be used as components for explosive mixtures.[37] The reactions described herein were only run on a few grams scale and no problems were encountered. However, *great caution* should be exercised when handling, knocking or heating compounds of this

type. Following the general method reported by Koguro and co-workers,[38] [H-**iQTZ**] was obtained in quantitative yield. [H-**iQTZ**] ^{1}H-NMR (DMSO d^6, 400 MHz) δ (ppm) = 9.34 (d, $J_{H\text{-}H}$ = 8.79 Hz, 1H, H10), 8.72 (d, $J_{H\text{-}H}$ = 5.59 Hz, 1H, H4), 8.14-8.09 (m, 2H, H9, H6), 7.90-7.85 (m, 2H, H5, H7).

iQTZ-PPG. The preparation of **iQTZ-PPG** was accomplished by slightly modifying a previously reported procedure.[39] In a 50 mL, two neck round bottomed flask equipped with a stirring bar, iQTZ-H (1 eq.) was dissolved in 10 mL of an acetone/Et_3N (1.1 eq.) mixture. Then, a solution of propargyl bromide (1 eq.) in 5 mL of acetone was added dropwise over a period of 10 minutes and the resulting solution was refluxed for 2h. After cooling to r.t., the white precipitate formed was filtered off, and the crude was purified by column chromatography over SiO_2 eluted with EtoAc/EP 6:4, affording the N2-propargyl product as the second fraction. Yield: 0.98 g, 4.26 mmol, 82 %; N-4 : N-3 ratio 7:3. **iQTZ-PPG** (N-3), **^{1}H NMR**, 400 MHz, $CDCl_3$, δ (ppm) = 9.13 – 9.06 (m, 1H, H10), 8.72 (d, $J_{H\text{-}H}$= 5.6 Hz, 1H, H4), 7.91 – 7.87 (m, 1H, H9), 7.83 – 7.66 (m, 3H, H7, H6, H5), 5.57 (d, $J_{H\text{-}H}$= 2.6 Hz, 2H, H11, H12 CH_2), 2.61 (t, $J_{H\text{-}H}$= 2.6 Hz, 1H, H13, CH). **^{13}C{^{1}H} NMR** 100 MHz, $CDCl_3$, δ (ppm) = 165.31(Ct), 145.90 (C2), 142.42 (C10), 136.96 (C8), 130.59 (C6), 128.58 (C5), 127.20 (C7), 126.85 (C3), 126.80 (C4), 122.80 (C9), 76.42 (C12, -*C*≡CH), 73.71 (C13, -C≡*C*H), 43.06 (C11, -CH_2).

(npy) was obtained by standard Suzuki-Miyaura[40] coupling conditions between 2-bromopyridine and naphthalene 2-boronic acid pinacol ester in presence of [Pd(pph_3)$_4$] and K_2CO_3 in THF/H_2O. Yield: 0.34 g, 1.65 mmol, 84 %. **npy ^{1}H NMR**, 400 MHz, $CDCl_3$, δ (ppm) = 8.78-8.76 (m, 1H), 8.50 (m, 1H), 8.17-8.14 (dd, $J_{H\text{-}H}$ = 1.99, $J_{H\text{-}H}$ = 6.79, 1H), 7.96-7.94 (m, 2H), 7.89-7.83 (m, 2H), 7.77-7.29 (m, 1H), 7.53-7.50 (m, 2H), 7.25-7.22 (m, 1H).

Dichlorobridged Ir(III) dimers were obtained according to the Nonoyama protocol, by combining $IrCl_3$*3.08 H_2O and a cyclometalating ligand (ppy or npy) in ethoxyethanol/H_2O 3:1 mixture, under argon atmosphere at 130°C for 24h.[41]

General Procedure for the synthesis of [Ir(C^N)$_2$(iQTZ-PPG)][PF$_6$]-type complexes. In a 50 mL two neck round bottom flask equipped with a stirring bar, [Ir(C^N)$_2$Cl]$_2$ (1 eq.) and **iQTZ-PPG** (2.5 eq.) were dissolved in a 20 mL DCM/EtOH 3:1 mixture, then stirred at r.t. for 6h. Anion metathesis was carried out by adding an excess of NH_4PF_6 to the solution and stirring for 20 minutes. The product was then extracted using dichloromethane (3 × 10 mL) and the organic components were combined and dried over anhydrous $MgSO_4$. Subsequent purification by column chromatography over SiO_2 (CH_2Cl_2/Acetone 9:1 to 7:3) yielded the desired Ir(III) complex as second fraction. Yield: **[Ir(ppy)$_2$(iQTZ-PPG)]$^+$** = 0.096 g, 0.109 mmol, 85%; **[Ir(npy)$_2$(iQTZ-PPG)]$^+$** = 0.070 g, 0.071 mmol, 91%.

[Ir(ppy)$_2$(iQTZ-PPG)]$^+$ ^{1}H NMR (400 MHz, Acetone-d_6) δ (ppm) = 9.61 – 9.55 (m, 1H), 8.29 – 8.21 (m, 4H), 8.16 – 8.04 (m, 4H), 8.00 – 7.91 (m, 3H), 7.91 – 7.84 (m, 2H), 7.13 – 7.05 (m, 3H), 7.05 – 6.93 (m, 2H), 6.88 (m, 1H), 6.38 – 6.31 (m, 2H), 5.96 (t, $J_{H\text{-}H}$= 2.7 Hz, 2H, CH_2), 3.42 (t, $J_{H\text{-}H}$= 2.6 Hz, 1H, ≡CH). **^{13}C{^{1}H} NMR** (100 MHz, Acetone-d_6) δ (ppm) = 168.01 (C_t), 167.82 (C-Ir), 167.25 (C-Ir), 150.36, 150.04, 148.89, 144.76, 144.42, 144.33, 144.17, 142.19, 138.87, 138.82, 137.17, 133.50, 131.91, 131.44, 131.26, 130.50, 129.75, 128.27, 128.12, 127.02, 125.59, 125.03, 124.54, 123.58, 123.49, 122.96, 122.51, 119.86, 119.76, 78.19 (-*C*≡CH), 73.29 (-C≡*C*H), 45.28 (CH_2). **ESI-MS** (m/z), CH_3CN = $[M]^+$ = 736; $[M]^-$ = 145 (PF_6). Anal. Calc. for $C_{35}H_{25}N_7F_6P_1Ir_1$ (880.8): C 47.73, H 2.86, N 11.13. Found: C 47.69, H 2.87, N 11.15%

[Ir(npy)$_2$(iQTZ-PPG)]$^+$ ^{1}H NMR (400 MHz, Acetone-d_6) δ (ppm) = 9.60 – 9.58 (m, 2H), 8.55 – 8.42 (m, 4H), 8.30 – 7.95 (m, 8H), 7.83 – 7.72 (m, 4H), 7.44 – 7.25 (m, 6H), 6.71 – 6.74 (m, 2H), 6.12 – 6.05 (m, 2H, CH_2), 3.38 (m, 1H, ≡CH). **^{13}C{^{1}H} NMR** (100 MHz, Acetone-d_6) δ (ppm) = 168.13 (C_t), 166.99 (C-Ir), 166.48 (C-Ir), 150.68, 150.40, 144.49, 144.36, 143.98, 142.97, 142.2, 138.87, 138.84, 138.56, 137.23, 135.43, 135.09, 133.47, 131.42, 130.68, 130.61, 129.18, 129.18, 128.88, 128.73, 128.67, 128.27, 128.22, 127.07, 127.06, 126.80, 125.97, 125.84, 125.74, 125.62, 124.70, 124.37, 124.34, 124.11, 124.02, 123.70, 120.66, 78.16 (-*C*≡CH), 73.25 (-C≡*C*H), 45.27 (CH_2). **ESI-MS** (m/z), CH_3CN = $[M]^+$ = 837; $[M]^-$ = 145 (PF_6). Anal. Calc. for $C_{43}H_{29}N_7F_6P_1Ir_1$ (980.92): C 52.65, H 2.98, N 10.0. Found: C 52.60, H 3.01, N 9.98%

Electronic Supporting Information (ESI †) available: ESI-MS, ^{1}H and ^{13}C NMR spectra; Absorption, Excitation and Emission spectra; PBzMA doped film appearance and LSCs transmittance profiles in PMMA and PCHMA; Photostability of Ir(III) complexes embedded into PMMA; W/V Curves for PV cells and LSC+PV cells.

Conflicts of Interests. There are no conflicts to declare.

Acknowledgments. The financial support from the University of Pisa (PRA_2020_21 – SUNRISE) and the Italian Ministry of Education, University and Research (PRIN project: Towards a Sustainable Chemistry: Design of Innovative Metal-Ligand Systems for Catalysis and Energy Applications) is gratefully acknowledged. The authors also express their gratitude for a grant (to N.M.) funded by the Marco Polo program joint by University of Bologna and the Curtin University of Perth.

Graphical Abstract

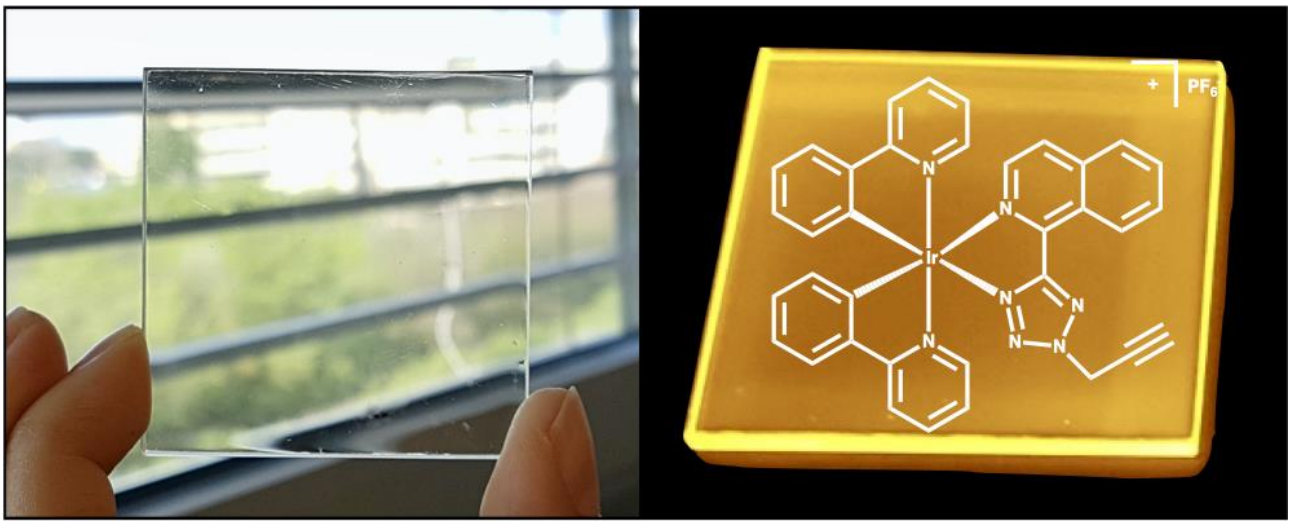

Synopsis: Phosphorescent Ir(III) complexes make their debut in LSC technology with the preparation of Ir(III)-doped colourless luminescent solar concentrators.

References

[1] a) L. Flamigni, A. Barbieri, C. Sabatini, B. Ventura and F. Barigelletti, "Photochemistry and Photophysics of Coordination Compounds: Iridium", *Top. Curr. Chem*., **2007**, *281*, 143–203. https://doi.org/10.1007/128_2007_131; b) F. Puntoriero, F. Nastasi, M. Galletta and S. Campagna, "8.07 - Photophysics and Photochemistry of Non-Carbonyl-Containing Coordination and Organometallic Compounds", *Comprehensive Inorganic Chemistry II (Second Edition)*, **2013**, *8*, 255–337. https://doi.org/10.1016/B978-0-08-097774-4.00802-0.

[2] J. C. Deaton and F. N. Castellano, "Archetypal Iridium(III) Compounds for Optoelectronic and Photonic Applications: Photophysical Properties and Synthetic Methods" In Iridium(III) in Optoelectronic and Photonics Applications; E. Zysman-Colman, Ed. Wiley-VHC:Weinheim, Germany, **2017**, 1−70 and references cited herein. https://doi.org/10.1002/9781119007166.

[3] a) K. K-W. Lo and K. Y. Zhang, "Iridium(III) complexes as therapeutic and bioimaging reagents for cellular applications", *RSC Adv*., **2012**, *2*, 12069-12083. https://doi.org/10.1039/C2RA20967E. b) C. Caporale and M. Massi, "Cyclometalated Iridium(III) complexes for life science", *Coord. Chem. Rev.*, **2018**, *363*, 71–91. https://doi.org/10.1016/j.ccr.2018.02.006.

[4] a) D. A. Nicewicz and D. W. C. MacMillan, "Merging Photoredox Catalysis with Organocatalysis: The Direct Asymmetric Alkylation of Aldehydes", *Science*, **2008**, *322*, 77–80. https://doi.org/10.1126/science.1161976. b) C. K. Prier, D. A. Rankic and D. W. C. MacMillan, "Visible Light Photoredox Catalysis with Transition Metal Complexes: Applications in Organic Synthesis", *Chem. Rev.,* **2013**, *113*, 5322-5363. https://doi.org/10.1021/cr300503r.

[5] a) B. P. Fors and C. J. Hawker, "Control of a Living Radical Polymerization of Methacrylates by Light", *Angew. Chem. Int. Ed.*, **2012**, *51*, 8850 – 8853. https://doi.org/10.1002/anie.201203639; b) J. Lalevée, M. Peter, F. Dumur, D. Gigmes, N. Blanchard, M-A. Tehfe, F. Morlet-Savary and J. P. Fouassier, "Subtle Ligand Effects in Oxidative Photocatalysis with Iridium Complexes: Application to Photopolymerization", *Chem. Eur. J.,* **2011**, *17*, 15027 – 15031. https://doi.org/10.1002/chem.201101445.

[6] C-L. Ho and W-Y. Wong, "Metal-containing polymers: Facile tuning of photophysical traits and emerging applications in organic electronics and photonics", *Coord. Chem. Rev.*, **2011**, *255*, 2469-2502. https://doi.org/10.1016/j.ccr.2011.01.052.

[7] E. Holder, V. Marin, D. Kozodaev, M. A. R. Meier, B. G. G. Lohmeijer, and U. S. Schubert, "Iridium(III) Complexes with PEO and PS Polymer Macroligands and Light-Emitting Properties: Synthesis and Characterization", *Macromol. Chem. Phys.* **2005**, *206*, 989–997. https://doi.org/10.1002/macp.200400544.

[8] F. Xu, H. U. Kima, J-H. Kima, B. J. Jung, A. C. Grimsdale and D-H. Hwang, "Progress and perspective of iridium-containing phosphorescent polymers for light-emitting diodes", *Prog. Polym. Sci.*, **2015**, *47*, 92-121. http://dx.doi.org/10.1016/j.progpolymsci.2015.01.005.

[9] a) M. G. Debije and P. P. C. Verbunt, "Thirty Years of Luminescent Solar Concentrator Research: Solar Energy for the Built Environment", *Adv. Energy Mater.*, **2012**, *2*, 12-35. https://doi.org/10.1002/aenm.201290003; b) F. Meinardi, F. Bruni and S. Brovelli, "Luminescent solar concentrators for building-integrated photovoltaics", *Nat. Rev. Mater.*, **2017**, *2*, 17072. https://doi.org/10.1038/natrevmats.2017.72. c) G. Griffini, M. Levi and S. Turri, "Thin-film luminescent solar concentrators: A device study towards rational design", *Renewable Energy*, **2015**, *78*, 288-294. https://doi.org/10.1016/j.renene.2015.01.009; see also: d) G. Griffini, "Host Matrix Materials for Luminescent Solar Concentrators: Recent Achievements and Forthcoming Challenges", *Front. Mater.,* **2019**, *6*, 29. https://doi.org/10.3389/fmats.2019.00029.

[10] a) G. Albano, T. Colli, L. Nucci, R. Charaf, T. Biver, A. Pucci and L. A. Aronica, "Synthesis of new bis[1-(thiophenyl)propynones] as potential organic dyes for colorless luminescent solar concentrators (LSCs)", *Dyes Pigm.*, **2020**, *174*, 108100. https://doi.org/10.1016/j.dyepig.2019.108100; b) F. Bellina, C. Manzini, G. Marianetti, C. Pezzetta, E. Fanizza, M. Lessi, P. Minei, V. Barone and A. Pucci, "A Colourless p-phenylene-spaced bis-azoles for luminescent concentrators", *Dyes Pigm.*, **2016**, *134*, 118-128. https://doi.org/10.1016/j.dyepig.2016.07.005.

[11] C. Yang C and R. R. Lunt, "Limits of visibly transparent luminescent solar concentrators", *Adv. Opt. Mater.*, **2017**, *5*, 1600851. https://doi.org/10.1002/adom.201600851.

[12] a) S. Stagni, S. Colella, A. Palazzi, G. Valenti, S. Zacchini, F. Paolucci, M. Marcaccio, R. Q. Albuquerque and L. De Cola "Essential Role of the Ancillary Ligand in the Color Tuning of Iridium Tetrazolate Complexes", *Inorg. Chem*., **2008**, *47*, 10509–10521. https://doi.org/10.1021/ic801157k. see also: b) V. Fiorini, A. D'Ignazio, K. D. M. Magee, M. I. Ogden, M. Massi and S. Stagni "Fully Ir(III) tetrazolate soft salts: the road to white-emitting ion pairs", *Dalton. Trans*, **2016**, *45*, 3256 – 3259. https://doi.org/10.1039/C5DT04958J; c) A. M. Ranieri, C. Caporale, V. Fiorini, A. Hubbard, P. Rigby,

S. Stagni, E. Watkin, M. I. Ogden, M. J. Hackett, and M. Massi, "Complementary Approaches to Imaging Subcellular Lipid Architectures in Live Bacteria Using Phosphorescent Iridium Complexes and Raman Spectroscopy", *Chem. Eur. J.*, **2019**, *25*, 10566 –10570. https://doi.org/10.1002/chem.201902023.

[13] S. F. H. Correia, V. de Zea Bermudez, S. J. L. Ribeiro, P. S. Andrè, R. A. S. Ferreira and L. D. Carlos, "Luminescent solar concentrators: challenges for lanthanide-based organic–inorganic hybrid materials", *J. Mater. Chem. A*, **2014**, *2*, 5580–5596. https://doi.org/10.1039/C3TA14964A.

[14] a) C. Caporale, C. A. Bader, A. Sorvina, K. D. M. MaGee, B. W. Skelton, T. A. Gillam, P. J. Wright, P. Raiteri, S. Stagni, J. L. Morrison, S. E. Plush, D. A. Brooks, and M. Massi, "Investigating Intracellular Localisation and Cytotoxicity Trends for Neutral and Cationic Iridium Tetrazolato Complexes in Live Cells", *Chem. Eur. J.* **2017**, *23*, 15666 – 15679. https://doi.org/10.1002/chem.201701352; b) V. Fiorini, S. Zacchini, P. Raiteri, R. Mazzoni, V. Zanotti, M. Massi and S. Stagni, "Negatively charged Ir(III) cyclometalated complexes containing a chelating bis-tetrazolato ligand: synthesis, photophysics and the study of reactivity with electrophiles", *Dalton. Trans.,* **2016***, 45*, 12884-12896. https://doi.org/10.1039/C6DT02524B; c) V. Fiorini, I. Zanoni, S. Zacchini, A. L. Costa, A. Hochkoeppler, V. Zanotti, A. M. Ranieri, M. Massi, A. Stefan and S. Stagni "Methylation of Ir(III)-tetrazolato complexes: an effective route to modulate the emission outputs and to switch to antimicrobial properties", *Dalton. Trans.,* **2017**, *46,* 12328-12338. https://doi.org/10.1039/C7DT02352A; see also: d) N. Monti, S. Zacchini, M. Massi, A. Hochkoeppler, L. Giorgini, V. Fiorini, A. Stefan and S. Stagni "Antibacterial activity of a new class of tris homoleptic Ru (II)-complexes with alkyl-tetrazoles as diimine-type ligands", *Appl. Organomet. Chem.*, **2020**, *34*, e5806. https://doi.org/10.1002/aoc.5806; e) N. Monti, V. Longo, S. Zacchini, G. Vigarani, L. Giorgini, E. Bonora, M. Massi, V. Fiorini and S. Stagni, "Alkyl tetrazoles as diimine ("diim") ligands for *fac*-[Re(diim)$(CO)_3$(L)]-type complexes. Synthesis, characterization and preliminary studies of the interaction with bovine serum albumin", *Inorg. Chim. Acta*, **2021**, *518*, 120244. https://doi.org/10.1016/j.ica.2020.120244

[15] M. V. Werrett, S. Muzzioli, P. J. Wright, A. Palazzi, P. Raiteri, S Zacchini, M. Massi and S. Stagni "Proton-Induced Reversible Modulation of the Luminescent Output of Rhenium(I), Iridium(III), and Ruthenium(II) Tetrazolate Complexes", *Inorg. Chem.*, **2014**, *53*, 1, 229–243. https://doi.org/10.1021/ic402187e.

[16] K. Nakamaru ”Synthesis, Luminescence Quantum Yields, and Lifetimes of Trischelated Ruthenium(II) Mixed-ligand Complexes Including 3,3′-Dimethyl-2,2′-bipyridyl”, Bull. Chem. Soc. Jpn., **1982**, *55*, 2697–2705. https://doi.org/10.1246/bcsj.55.2697.

[17] a) F. J. Ostos, G. Iasilli, M. Carlotti and A. Pucci "High-Performance Luminescent Solar Concentrators Based on Poly(Cyclohexylmethacrylate) (PCHMA) Films”, *Polymers*, **2020**, *12*, 2898. https://doi.org/10.3390/polym12122898; b) C. Papucci, A. Dessì, C. Coppola, A. Sinicropi, G. Santi, M. Di Donato, M. Taddei, P. Foggi, L. Zania, G. Reginato, A. Pucci, M. Calamante and A. Mordini "Benzo[1,2-d:4,5-d′]bisthiazole fluorophores for luminescent solar concentrators: synthesis, optical properties and effect of the polymer matrix on the device performances”, *Dyes Pigments*, **2021**, *188*, 109207. https://doi.org/10.1016/j.dyepig.2021.109207.

[18] P. Minei, G. Iasilli, G. Ruggeri and A. Pucci ”Luminescent Solar Concentrators from Waterborne Polymer Coatings”, *Coatings*, **2020**, *10*, 655. https://doi.org/10.3390/coatings10070655.

[19] J. Roncali “Luminescent Scolar Collectors: Quo Vadis?”, *Adv. Energy Mater*., **2020**, *10*, 2001907. https://doi.org/10.1002/aenm.202001907.

[20] S. Mattiello, A. Sanzone, F. Bruni, M. Gandini, V. Pinchetti, A. Monguzzi, I. Facchinetti, R. Ruffo, F. Meinardi, G. Mattioli, M. Sassi, S. Brovelli and L. Beverina, “Chemically Sustainable Large Stokes Shift Derivatives for High-Performance Large-Area Transparent Luminescent Solar Concentrators”, *Joule,* **2020**, *4*, 1988–2003. https://doi.org/10.1016/j.joule.2020.08.006.

[21] C. Yang, W. Sheng, M. Moemeni, M. Bates, C. K. Herrera, B. Borhan and R. R. Lunt, “Ultraviolet and Near-Infrared Dual-Band Selective-Harvesting Transparent Luminescent Solar Concentrators”, *Adv. Energy Mater*., **2021**, *11*, 2003581. https://doi.org/10.1002/aenm.202003581.

[22] G. A. Crosby and J. N. Demas, “Measurement of photoluminescence quantum yields. Review.”, *J. Phys. Chem.*, **1971**, *75*, 991-1024. https://doi.org/10.1021/j100678a001.

[23] F. Eaton, “Reference materials for luminescence measurements”, *Pure Appl. Chem*., **1988**, *60*, 1107-1114.

[24] T. A. Geervliet, I. Gavrila, G. Iasilli, F. Picchioni and A. Pucci, “Luminescent Solar Concentrators Based on Renewable Polyester Matrices”, *Chem. Asian J.*, **2019**, *14*, 877-883. https://doi.org/10.1002/asia.201801690.

[25] R. Mori, G. Iasilli, M. Lessi, A. B. Munoz-Garcia, M. Pavone, F. Bellina and A. Pucci, “Luminescent solar concentrators based on PMMA films obtained from a red-emitting ATRP initiator”, *Polym. Chem.*, **2018**, *9*, 1168-1177. https://doi.org/10.1039/C7PY01933E. b) M. G. Debije, R. C. Evans and

G. Griffini “Laboratory protocols for measuring and reporting the performance of luminescent solar concentrators”, *Energy Environ. Sci.*, **2021**, *14*, 293. https://doi.org/10.1039/D0EE02967J.

[26] a) M. Lucarelli, C. Lessi, P. Manzini, F. Minei, F. Bellina and A. Pucci, “N-alkyl diketopyrrolopyrrole-based fluorophores for luminescent solar concentrators: Effect of the alkyl chain on dye efficiency”, *Dyes Pigm.*, **2016**, *135*, 154-162. https://doi.org/10.1016/j.dyepig.2016.03.036. b) G. Iasilli, R. Francischello, P. Lova, S. Silvano, A. Surace, G. Pesce, M. Alloisio, M. Patrini, M. Shimizu, D. Comoretto and A. Pucci, “Luminescent solar concentrators: boosted optical efficiency by polymer dielectric mirrors”, *Mater. Chem. Front.*, **2019**, *3*, 429-436. https://doi.org/10.1039/C8QM00595H. c) F. De Nisi, R. Francischello, A. Battisti, A. Panniello, E. Fanizza, M. Striccoli, X. Gu, N. L. C. Leung, B. Z. Tang and A. Pucci, “Red-emitting AIEgen for luminescent solar concentrators”, *Mater. Chem. Front.*, **2017**, *1*, 1406 – 1412. https://doi.org/10.1039/C7QM00008A. d) M. Carlotti, E. Fanizza, A. Panniello and A. Pucci, “A fast and effective procedure for the optical efficiency determination of luminescent solar concentrators”, *Solar Ener.*, **2015**, *119*, 452-460. https://doi.org/10.1016/j.solener.2015.05.031.

[27] F. Gianfaldoni, F. De Nisi, G. Iasilli, A. Panniello, E. Fanizza, M. Striccoli, D. Ryuse, M. Shimizu, T.Biver and A. Pucci, “A push–pull silafluorene fluorophore for highly efficient luminescent solar concentrators”, *RSC Adv.*, **2017**, *7*, 37302-37309. https://doi.org/10.1039/C7RA08022K.

[28] M. Sottile, G. Tomei, S. Borsacchi, F. Martini, M. Geppi, G. Ruggeri and A. Pucci, “Epoxy resin doped with Coumarin 6: Example of accessible luminescent collectors”, *Eur. Polym. J.*, **2017**, *89*, 23-33. https://doi.org/10.1016/j.eurpolymj.2017.02.003.

[29] C. Yang, D. Liu and R. R. Lunt, “How to Accurately Report Transparent Luminescent Solar Concentrators”, *Joule*, **2019**, *3*, 2871-2883. https://doi.org/10.1016/j.joule.2019.10.009.

[30] M. J. Frisch, G. W. Trucks, H. B. Schlegel, G. E. Scuseria, M. A. Robb, J. R. Cheeseman, G. Scalmani, V. Barone, G. A. Petersson, H. Nakatsuji, X. Li, M. Caricato, A. V. Marenich, J. Bloino, B. G. Janesko, R. Gomperts, B. Mennucci, H. P. Hratchian, J. V. Ortiz, A. F. Izmaylov, J. L. Sonnenberg, D. Williams-Young, F. Ding, F. Lipparini, F. Egidi, J. Goings, B. Peng, A. Petrone, T. Henderson, D. Ranasinghe, V. G. Zakrzewski, J. Gao, N. Rega, G. Zheng, W. Liang, M. Hada, M. Ehara, K. Toyota, R. Fukuda, J. Hasegawa, M. Ishida, T. Nakajima, Y. Honda, O. Kitao, H. Nakai, T. Vreven, K. Throssell, J. A. Montgomery, Jr., J. E. Peralta, F. Ogliaro, M. J. Bearpark, J. J. Heyd, E. N. Brothers, K. N. Kudin, V. N. Staroverov, T. A. Keith, R. Kobayashi, J. Normand, K. Raghavachari, A. P. Rendell, J. C. Burant, S. S. Iyengar, J. Tomasi, M. Cossi, J. M. Millam, M. Klene, C. Adamo, R. Cammi, J. W. Ochterski, R. L.

Martin, K. Morokuma, O. Farkas, J. B. Foresman, and D. J. Fox, "*Gaussian 16*, Revision C.01", *Gaussian, Inc., Wallingford CT*, 2016.

[31] C. Adamo and V. Barone, "Toward reliable density functional methods without adjustable parameters: The PBE0 model", *J. Chem. Phys.,* **1999**, *110*, 6158-69. https://doi.org/10.1063/1.478522.

[32] S. Grimme, S. Ehrlich and L. Goerigk, "Effect of the damping function in dispersion corrected density functional theory", *J. Comp. Chem.,* **2011**, *32*, 1456-65. https://doi.org/10.1002/jcc.21759.

[33] A. Bergner, M. Dolg, W. Kuechle, H. Stoll and H. Preuss, "Ab Initio Energy-adjusted Pseudopotentials for Elements of Groups 13− 17", *Mol. Phys.,* **1993**, *80,* 1431−1441. https://doi.org/10.1080/00268979300103121.

[34] G. A. Petersson, A. Bennett, T. G. Tensfeldt, M. A. Al-Laham, W. A. Shirley and J. A. Mantzaris, "Complete basis set model chemistry. I. The total energies of closed-shell atoms and hydrides of the first-row atoms", *J. Chem. Phys.*, **1988**, *89*, 2193-218. https://doi.org/10.1063/1.455064.

[35] V Criscuolo, C. T. Prontera, M. Pavone, O. Crescenzi, M. G. Maglione, P. Tassini, S. Lettieri, P. Maddalena, C. Borriello, C. Minarini and P. Manini, "Luminescent cis-Iridium(III) Complex Based on a Bis(6,7-dimethoxy-3,4-dihydroisoquinoline) Platform Featuring an Unusual cis Orientation of the CΛN Ligands: From a Theoretical Approach to a Deep Red LEEC Device", *ACS Omega*, **2019**, *4*, 1, 2009-2018. https://doi.org/10.1021/acsomega.8b02859.

[36] G. Scalmani and M. J. Frisch, "Continuous Surface Charge Polarizable Continuum Models of Solvation. I. General Formalism", *J. Chem. Phys.*, **2010**, *132*, 114110. https://doi.org/10.1063/1.3359469.

[37] R. N. Butler, "Tetrazoles, Comprehensive Heterocyclic Chemistry II"; Storr, R. C., Ed.; Pergamon Press: Oxford, U.K., **1996**, *4*, 621-678, and references cited therein.

[38] K. Koguro, T. Oga, S. Mitsui and R. Orita, "Novel Synthesis of 5-Substituted Tetrazoles from Nitriles", *Synthesis*, **1998**, 910-914. https://doi.org/10.1055/s-1998-2081.

[39] L. I. Vereshchagin, A. V. Maksikova, L. G. Tikhonova, S. R. Buzilova and G. V. Sakovich, "Synthesis of polynuclear uncondensed tri- and tetrazoles", *Chem. Heterocycl. Compd*., **1981**, *17*, 510-515. https://doi.org/10.1007/BF00505701.

[40] N. Miyaura and A. Suzuki, “Stereoselective synthesis of arylated (E)-alkenes by the reaction of alk-1-enylboranes with aryl halides in the presence of palladium catalyst”, *J. Chem. Soc., Chem. Commun.*, **1979**, *0*, 866-867. https://doi.org/10.1039/C39790000866.

[41] M. Nonoyama, “Benzo[h]quinolin-10-yl-N Iridium(III) Complexes”, *Bull. Chem. Soc. Jpn.*, **1974**, *47*, 767. https://doi.org/10.1246/bcsj.47.767.